A theoretical study of the mechanisms for 1,3-dipolar cycloadditions of diphenyldiazomethane to C60 and C70

ARTICLE *in* JOURNAL OF PHYSICAL ORGANIC CHEMISTRY · OCTOBER 2014

Impact Factor: 1.38 · DOI: 10.1002/poc.3342

2 AUTHORS, INCLUDING:

Cui Chengxing
Beijing Normal University
10 PUBLICATIONS **24** CITATIONS

SEE PROFILE

Research Article

Journal of Physical Organic Chemistry

Received: 9 May 2014, Revised: 9 July 2014, Accepted: 16 July 2014, Published online in Wiley Online Library: 8 August 2014

(wileyonlinelibrary.com) DOI: 10.1002/poc.3342

A theoretical study of the mechanisms for 1,3-dipolar cycloadditions of diphenyldiazomethane to C_{60} and C_{70}

Cheng-Xing Cui[a,b] and Ya-Jun Liu[a]*

The 1,3-dipolar cycloaddition (1,3-DPCA) reaction plays a crucial role during the functionalization of fullerenes, which have broad applications in the materials and pharmaceutical fields. In concert with previous experiments, we theoretically investigated the mechanisms of 1,3-DPCA of diphenyldiazomethane (DDMf) to two fullerenes (C_{60} and C_{70}) using the M06-2X density functional method under vacuum and in solvents. To understand the influence of the dipolarophile on these reactions, the 1,3-DPCA of DDMf to three common acceptors, specifically tetracyanoethylene (TCNE), 2,3-dichloro-5,6-dicyano-1,4-benzoquinone (DDQ), and chloranil (CA), was also studied at the same computational level. The substituent effects on the five reactions were investigated by modeling 1,3-DPCA reactions with 12 different substituted DDMf (DDMs) with five dipolarophiles, totaling 60 reactions. Including the five unsubstituted DDMf reactions, 65 1,3-DPCA reactions were studied. The stereoselectivity, relative reactivity, solvent effects, and distortion/interaction energy model were carefully considered and analyzed based on their corresponding electronic structures, electrostatic potential surfaces, interaction models, solvent models, and thermodynamic data. An intermediate was identified for each of the 65 reactions. A possible biradical pathway for the reactions between DDMf and the two fullerenes was also investigated. The calculated results corroborate and enrich the experimental observations. The conclusion and detailed discussion are generally important for understanding the 1,3-DPCA reactions to fullerenes.

Keywords: M06-2X; 1,3-dipolar cycloaddition; fullerenes

INTRODUCTION

Among the 30 or more forms of fullerenes, C_{60} and C_{70} are the most common representatives; both have been investigated frequently over the last 50 years. Their physicochemical properties and new applications are constantly surveyed. Friedman et al. examined the inhibition of an HIV-1 protease using C_{60} derivatives through a computational strategy.[1,2] The applications of C_{60} and C_{70} in materials and other fields have also been investigated extensively.[3–5] C_{60} has an I_h symmetry with equivalent carbon atoms and has two types of bonds, which are conventionally denoted 6—5 and 6—6 bonds.[6] The 6—6 bond is more reactive than the 6—5 bond.[7] Due to its lower (D_{5h}) symmetry, C_{70} contains five types of distinct carbon atoms and eight types of different C—C bonds.[8] The widely accepted nomenclature[8] is shown in Fig. 1. The eight types of bonds in C_{70} were classified by Scuseria[9] into three groups based on the nature of their bonds: double (a—b, c—c, and d—d), intermediate (d—e), and single bonds (a—a, b—c, e—e, and c—d).

After pericyclic reactions were discovered, they proved quite reliable and synthetically importance during the first half of the past century. These useful yet mysterious reactions are traditionally described as "no-mechanism" reactions because they involve no reactive intermediates (Int). 1,3-Dipolar cycloadditions (1,3-DPCA) are prototypical pericyclic reactions that are important during the functionalization of fullerenes. This reaction and the Diels–Alder (DA) reaction, which is another important pericyclic reaction, hold great promise for further applications in material and pharmaceutical applications for fullerenes.[10–25] Total regioselective control is essential when preparing fullerene derivatives. The nature of the C—C bonds in fullerenes strongly influences their reactivity. Cycloadditions to the C—C bonds of fullerenes are more facile when the C—C bond is shorter[14] because the shorter bonds possess larger π-bond orders and higher π-densities. Therefore, cycloadditions to C_{60} most likely to occur at the 6—6 bond,[13,26,27] while cycloadditions to C_{70} prefer the a—b, c—c, and d—d bonds.[26,28] Isobe's[29] and Ishi-I's[30] groups performed excellent research in this area. The 1,3-DPCA reaction is analogue to the DA reaction: they are both concerted [$\pi4_s + \pi2_s$] cycloadditions. Because many structures can serve as either a 1,3-dipole or a dipolarophile, the 1,3-DPCA is commonly used during the synthesis of five-membered heterocyclic rings. Oshima et al. investigated the kinetics of 1,3-DPCA reactions combining diphenyldiazomethane (DDMf in Fig. 1) with C_{60} and C_{70} in toluene at 30 °C and compared these reactions to the 1,3-DPCA of DDMf to tetracyanoethylene (TCNE), 2,3-dichloro-5,6-dicyano-1,4-benzoquinone (DDQ), and chloranil (CA).[31] They also experimentally explored the kinetic substituent effects based on

* *Correspondence to: Y.-J. Liu, Key Laboratory of Theoretical and Computational Photochemistry, Ministry of Education, College of Chemistry, Beijing Normal University, Beijing 100875, China.*
E-mail: yajun.liu@bnu.edu.cn

a *C.-X. Cui, Y.-J. Liu*
Key Laboratory of Theoretical and Computational Photochemistry, Ministry of Education, College of Chemistry, Beijing Normal University, Beijing 100875, China

b *C.-X. Cui*
School of Chemistry and Chemical Engineering, Henan Institute of Science and Technology, Xinxiang 453003, China

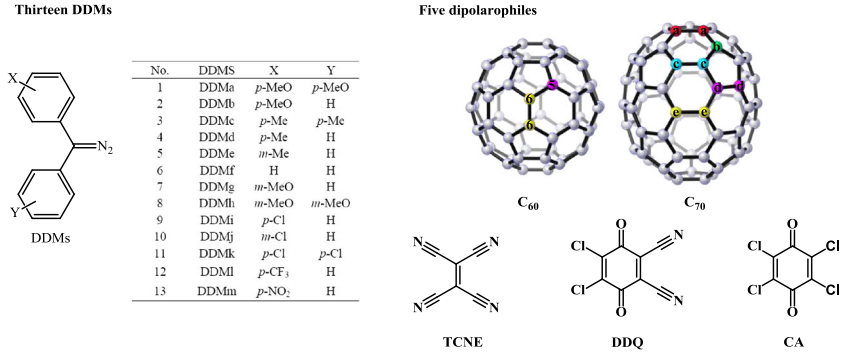

No.	DDMS	X	Y
1	DDMa	*p*-MeO	*p*-MeO
2	DDMb	*p*-MeO	H
3	DDMc	*p*-Me	*p*-Me
4	DDMd	*p*-Me	H
5	DDMe	*m*-Me	H
6	DDMf	H	H
7	DDMg	*m*-MeO	H
8	DDMh	*m*-MeO	*m*-MeO
9	DDMi	*p*-Cl	H
10	DDMj	*m*-Cl	H
11	DDMk	*p*-Cl	*p*-Cl
12	DDMl	*p*-CF_3	H
13	DDMm	*p*-NO_2	H

Figure 1. The structures of 13 DDMs, as well as C_{60}, C_{70}, TCNE, DDQ, and CA. The types of bonds in C_{60} and C_{70}

the 1,3-DPCA reactions between 12 derivatives of diphenyldiazomethane and five common acceptors. For convenience, we used DDMs to represent all of the unsubstituted and substituted diphenyldiazomethanes in the following text.

Combining theoretical studies with experimental observations provides detailed information regarding the reaction process and subsequently uncovers the reaction mechanism. In recent years, many theoretical studies have been performed on the 1,3-dipolar reactions and DA reactions with C_{60} and C_{70}. Among these theoretical calculations, the density functional theory (DFT) method was proved to be superior to the semi-empirical and HF methods.[7,26–28,32–35] Becke's three-parameter exchange with the nonlocal correlation of Lee, Yang, and Parr (B3LYP) is the most frequently used DFT function; it yields good thermodynamic data for simple DA reactions[36–39] and excellent geometries for curved polyarenes.[40] However, the B3LYP functional has a systematic error when used to predict the thermochemistry of DA reactions.[41,42] The hybrid meta-exchange-correlation functional M06-2X[43] was recommended for systems involving main-group thermochemistry, kinetics, non-covalent interactions, and electronic excitation energies for the valence and Rydberg states.[43] Numerous calculations in recent years indicate that the M06-2X functional is a reliable functional when studying cycloadditions to fullerenes and nanotubes.[11,44–46] We theoretically explored the cycloadditions of butadiene to C_{60} and C_{70} at the M06-2X/6-31G(d,p) computational level.[47] The calculated results indicated that the addition to the 6—6 bond using a Diels–Alder reaction is energetically more favorable than that with a 6—5 bond for C_{60}, while the addition to an a—b bond is the most facile for C_{70} both under vacuum and in toluene or CH_3CN, perfectly reproducing the experimental observations.[47] Due to the mechanistic similarities between the 1,3-DPCA and DA reactions, we predict that the 1,3-DPCA reactions of DDMs occur only at the 6—6 bond of C_{60} and a—b bond of C_{70}. For comparison, the 1,3-DPCA reactions of DDMs to TCNE, DDQ and CA were also studied on the same computational level.

Houk's group proposed a distortion/interaction model based on the 1,3-DPCA of nine 1,3-dipoles with ethylene and acetylene; the activation barriers for 1,3-DPCA reactions are intentionally divided into two imaginary categories concerning reaction strain distortions and electronic interactions.[48–50] After investigating the Diels–Alder reactions of four cycloalkenes with four dienes using the distortion/interaction model, they concluded that the reactivity of the dienes is controlled by both distortion and interaction energies.[51] Other cycloaddition systems were also rationalized using this model.[52–55,44,56] Another similar model is the so-called activation strain model;[57–61] when combined with the distortion/interaction model, we can obtain a quantitative comprehension of the physical factors that control the activation energy through different fundamental processes.

We now provide a comprehensive understanding of the reactions in the title. In Fig. 1, the structures of the DDMs and the five acceptors are shown, where each of the 13 DDMs will react with the acceptors, generating 65 reactions for the current study. The theories and concepts in physical organic chemistry are crucial for comprehending the mechanisms of organic reactions. Consequently, we systematically analyzed the computed results using different aspects of physical organic chemistry and compared these results to the experimental observation. Based on these analyses, we gained a better understanding of the 1,3-DPCA reactions between DDMf and C_{60} and C_{70}.

COMPUTATIONAL DETAILS

The basis sets 6-31G(d,p), 6-31 + G(d,p), 6-311G(d), and 6-311G(d,p) were tested for the 1,3-DPCA reactions of DDMf with TCNE, DDQ or CA using the M06-2X functional under vacuum based on the previous study.[62] According to Table S0, we can find that the basis sets negligibly affect thermodynamic data by the inclusion of diffusion function or changing from double zeta to triple zeta. Considering the compromise between chemical accuracy and computational cost, we optimized all the geometries at the M06-2X/6-31G(d,p) theoretical level[63] for the 65 1,3-DPCA reactions of the DDMs with the 6—6 bond of C_{60}, a—b bond of C_{70}, TCNE, DDQ, or CA under vacuum and in solution (toluene and CH_3CN). The vibrational frequency analysis was performed at the same level to confirm that the optimized structure was a minimum or a transition state (TS) and to obtain the zero-point energy. The effect of using toluene was modeled using the polarizable continuum model (PCM)[64] with a dielectric constant of 2.374. The effect of using CH_3CN was modeled using the conductor-like polarizable continuum model (CPCM) with a dielectric constant of 35.688.[65,66] ΔG_{Int}, ΔG^{TS}, and ΔG_{r} were used to denote the relative energy of Int, TS to the reactant, and the reaction heat in Gibbs free energy, respectively. $\Delta G^{\ddagger}$ represents the activation barrier from the Int to the product via the TS in Gibbs free energy. The corresponding entropy and enthalpy were denoted ΔS_{Int}, ΔS^{TS}, ΔS_{r}, and $\Delta S^{\ddagger}$, and by ΔH_{int}, ΔH^{TS}, ΔH_{r}, and $\Delta H^{\ddagger}$, respectively. The definitions of ΔG_{Int}, ΔG^{TS}, ΔG_{r}, and $\Delta G^{\ddagger}$ are $\Delta G_{Int} = G_{Int} - (G_{R1} + G_{R2})$, $\Delta G_{TS} = G_{TS} - (G_{RI} + G_{R2})$, $\Delta G_P = G_P - (G_{R1} + G_{R2})$, and $\Delta G^{\ddagger} = \Delta G_{\text{TS}} - \Delta G_{\text{Int}}$, where R1 denotes DDMs; R2 denotes C_{60}, C_{70}, TCNE, DDQ, or CA; and P denotes the product. The relative entropy and enthalpy values are defined in the same way as those of the Gibbs free energy.

According to the distortion/interaction model, the concerted TS geometry in the 1,3-DPCA reaction is obtained when the participating 1,3-dipole and the dipolarophile are distorted into the structures at the moment when they form the TS structure, and then the distorted reactants interact with each other to form the product. The distortion process is normally energetically unfavorable because the two reactants are no longer occupying their most stable structures, but the interaction energy is normally energetically favorable because the molecular orbitals match between the distorted reactants. The activation energy changes when varying the distortion and interaction energies. In essence, the processes of distortion and interaction are dependent upon each other; instead, they occur simultaneously during the entire process. The distortion energy can be

deconstructed into two parts: the distortion energy of the dipole ($\Delta E_{d,\ dipole}$), which is defined as $\Delta E_{d,\ dipole} = E$(deformed dipole in the geometry of the supermolecule) $- E$(dipole), and the distortion energy of the dipolarophile ($\Delta E_{d,\ dipolarophile}$), which is defined as $\Delta E_{d,\ dipolarophile} = E$(deformed dipolarophile in the geometry of the supermolecule) E(dipolarophile). The total distortion energy is the sum of $\Delta E_{d,\ dipole}$ and $\Delta E_{d,\ dipolarophile}$. Therefore, the two distorted reactants interact with each other. The interaction energy is ΔE_i. Briefly, the activation energy can be expressed as $\Delta E = \Delta E_{d,\ dipole} + \Delta E_{d,\ dipolarophile} + \Delta E_i$, where E is the electronic energy. All of our calculations were performed with the Gaussian 09 suite of programs.[67]

RESULTS AND DISCUSSION

The 1,3-DPCA reactions of DDMf with the five acceptors

The reaction pathways and the trapping of ints

The stereoselectivity was studied for the 1,3-DPCA reactions of DDMf with DDQ and CA. For DDQ or CA, the reaction occurs exclusively at the less hindered outer C=O group, generating labile 3-oxapyrazolines that quickly lose nitrogen to become betaine Ints.[68,69] Therefore, the reactions produce two possible stereoisomeric products: the *endo* and *exo* products. When combining DDQ with DDMf, the M062X/6-31G(d,p) calculated reaction channels and optimized geometries of Int, TS, and P are described in Fig. 2. The analogous information for the reaction of DDMf with CA is shown in Figure S1. The thermochemical data for the four pathways of the two reactions are listed in Table 1. Based on the calculated results in Table 1, the *exo* pathway is preferred for the 1,3-DPCA of DDQ to DDMf. Both the *endo* and *exo* pathways are exothermic by −15.5 and −10.4 kcal/mol, respectively. The activation barrier for the *endo* pathway is 16.7 kcal/mol higher than that of the *exo* pathway according to the Gibbs free energy. Moreover, the *endo* pathway is endergonic by 16.7 kcal/mol from reactant to product, but the *exo* channel is exergonic by 7.9 kcal/mol. The thermodynamic preference of the *exo* channel might originate from the steric and the π–π interaction. In the *endo* TS, the two phenyls on the DDMf are oriented right above the quinone ring. The two benzyl groups of DDMf and the benzyl cycle of DDQ move closer together when the reaction proceeds along the *endo* pathway. This steric hindrance increases the energy of the *endo* TS. The attacking of DDMf via the *exo* channel is easier because the two phenyl groups are oriented away from the quinone ring to avoid steric hindrance, facilitating the necessary collision. The other effect resembles a π–π interaction. Figure 3 shows the electrostatic potential surfaces of benzene as computed with the M062X/6-31G(d,p). Obviously, directly stacking two benzenes on top of each other will generate an adverse electrostatic repulsion between the negative electrostatic potential in the center of benzene, while the T-shape or displaced structure is less repulsive. Figure 4 shows the electrostatic potential surfaces of DDQ, CA, and DDMf, as well as those of the *endo* TS and *exo* TS. Unlike benzene, the center of the six-membered carbon ring in DDQ has positive electrostatic potential due to the strong electronegative effects of the chloride substituent and cyano group, while the centers of the two phenyl groups in DDMf have a negative electrostatic potential. DDMf and DDQ prefer a face-to-face interaction as they approach during the collision. However, the *endo* TS reveals that the six-membered carbon ring in DDQ interacts with the phenyl group of DDMf in a slip-stacked manner (see the top-view of the *endo* TS in Fig. 4), increasing the relative energy of the TS and making it energetically unfavorable. CA is similar to DDQ. Therefore, we only considered the *exo* channel during the discussion of the 1,3-DPCA reactions of DDQ or CA with DDMf.

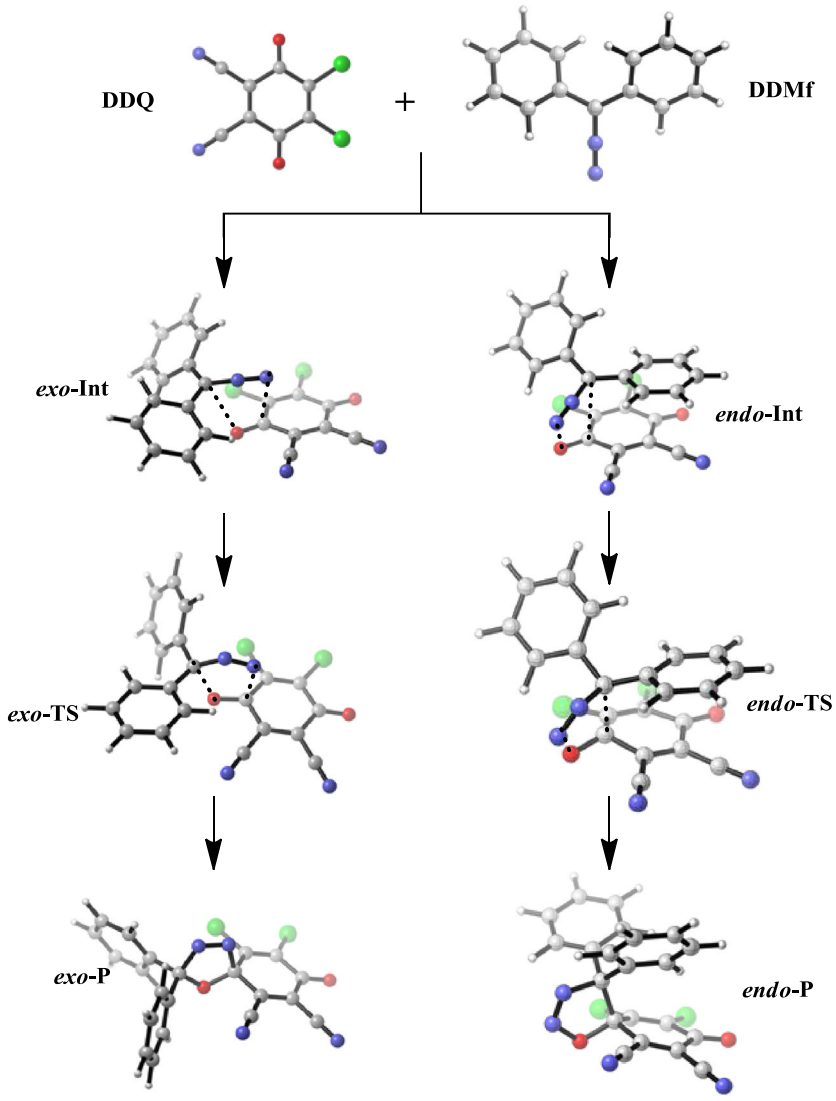

Figure 2. The *exo* and *endo* channels of the 1,3-DPCA reactions of DDQ and DDMf calculated at the M06-2X/6-31G(d,p) level under vacuum, where the gray, blue, red, and green balls represent the carbon, nitrogen, oxygen, and chlorine atoms, respectively

Table 1. The ΔS, ΔH, and ΔG of the 1,3-DPCA reactions of DDMf with DDQ, and DDMf with CA calculated at the M06-2X/6-31G(d,p) level under vacuum. (Unit: kcal/mol for ΔH and ΔG, e.u. for ΔS, where e.u. = cal/(K·mol))

	Int			TS			Activation barrier			P		
	ΔS_{Int}	ΔH_{Int}	ΔG_{Int}	ΔS_{TS}	ΔH_{TS}	ΔG_{TS}	$\Delta S^{‡}$	$\Delta H^{‡}$	$\Delta G^{‡}$	ΔS_r	ΔH_r	ΔG_r
DDQ/*endo*	−42.3	−15.5	−2.9	−56.8	9.4	26.3	−14.5	24.9	29.2	−54.3	0.6	16.7
DDQ/*exo*	−40.8	−10.4	1.8	−50.5	0.6	15.6	−9.7	11.0	13.9	−51.5	−23.3	−7.9
CA/*endo*	−46.8	−13.9	0.1	−56.6	14.5	31.4	−9.9	28.4	31.3	−53.8	3.1	19.2
CA/*exo*	−33.8	−7.3	2.8	−49.6	6.7	21.5	−15.8	14.0	18.7	−47.7	−21.5	−7.2

The 1,3-DPCA of DDMf with TCNE, C_{60} and C_{70} was studied. TCNE reacts with DDMf at its electron-deficient central C=C double bond.[70] For the 1,3-DPCA of the two fullerenes with DDMf, as mentioned in the Introduction, we only considered the 6—6 and a—b bonds. The major optimized parameters for the reactants, Ints, TSs, and products of the 1,3-DPCA of DDMf with C_{60}, C_{70}, TCNE, DDQ (the *exo* channel), and CA (the *exo* channel) are collected in Table 2. The Cartesian coordinates of these structures are listed in the supplementary information. The optimized geometries of the reactants, Int, TS, and product of the 1,3-DPCA reaction of DDMf and 6−6 bond of C_{60} are shown in Fig. 5. The other four reactions have pathways similar to that of C_{60} and are shown in Figure S2. The Ints between the reactants and the TSs are reported for the first time. However, we could not locate the TS between the reactant and the Int. The located Ints could be reactant complexes.

In summary, due to the large driving force, low steric hindrance, and more favorable electrostatic potential interactions, the 1,3-DPCA reactions of DDQ or CA with DDMf follow the *exo* reaction pathway. The 1,3-DPCA reactions between the five acceptors and DDMf have similar reaction pathways: two participating reactants combine to give the Int before overcoming a relative high activation barrier to form the product. An Int was located in each of the five reactions, indicating that pericyclic reactions, including 1,3-DPCA, are not "no-mechanism" reactions.

Geometric changes along the reaction coordinate

As shown in Table 2 and Fig. 5, the lengths of the C—C single bond formed (r_1 and r_2 of the Int) are 3.176 and 3.117 Å for the reaction of DDMf and C_{60}. The long bond distances reveal the weak interaction between the DDMf and C_{60}, as observed from the identical r_i (C—C distance between the two attacked carbon atoms) (1.387 Å) in the reactant and Int. During the reaction, the Int forms a five-membered C-C-C-N-N TS. The r_i is elongated to 1.443 Å, while r_1 and r_2 are shortened to 2.235 Å and 2.088 Å, respectively. Afterwards, the fused-ring product forms as r_i increases further and both r_1 and r_2 decrease. The r_1 and r_2 are different in the Int, TS, and product. There is no Int between the TS and product; therefore, the reaction is concerted and asynchronous. The geometric changes for the reaction of C_{70} and DDMf are similar. The r_1 and r_2 are 3.100 and 2.800 Å for TCNE, 2.848 and 2.776 Å for DDQ, and 3.074 and 2.766 Å for CA, respectively. The reaction of DDMf and TCNE passes through a five-membered C—C—C—N—N ring TS, while the reaction between DDMf and DDQ (or CA) utilizes five-membered C—C—O—N—N ring TSs to generate the products. Because oxygen is more electronegative than carbon, the r_i values of the Ints, TSs, and products of DDQ and CA are shorter than the analogous values for TCNE and DDMf.

Thermodynamic analysis

The calculated ΔS, ΔH, and ΔG of the five reactions are listed in Table 3. According to the geometry of the Int, C_{60} and DDMf do not form the C—C and the C—N bonds completely and bind tightly, which is reflected by the small ΔH_{Int} (−7.0 kcal/mol). When C_{60} and DDMf generate the product, the C—C and the C—N bonds have formed, and the ΔH_r (−17.1 kcal/mol) has a larger negative value. The ΔS_{Int} (−36.2 e.u.), ΔS_{TS} (−45.4 e.u.) and ΔS_R (−54.4 e.u.) values clearly reflect the changes in the degrees of freedom. The 3.8 kcal/mol ΔG_{Int} indicates that the change from the reactants to the Int is not favorable but is exothermic. The ΔG_r is −0.9 kcal/mol, revealing a spontaneous and exergonic process. From the Int to the product, the reaction must overcome a 16.9 kcal/mol activation energy barrier. The other four reactions have a reaction process similar to that between C_{60} and DDMf. The $\Delta G^{‡}$ values are 16.9, 15.8, 14.6, 13.9, and 18.7 kcal/mol for the reactions of DDMf and C_{60}, C_{70}, TCNE, DDQ, and CA, respectively. The $\Delta G^{‡}$ values occur in the following order: CA > C_{60} > C_{70} > TCNE DDQ. The ΔG_r values are −0.9, −1.1, −1.3, −7.9, and −7.2 kcal/mol for the reactions of DDMf with C_{60}, C_{70}, TCNE, DDQ, and CA, respectively. The order of the absolute value of ΔG_r is as follows: DDQ > CA > TCNE > C_{70} > C_{60}. The ΔH_r and ΔG_r for the reaction with

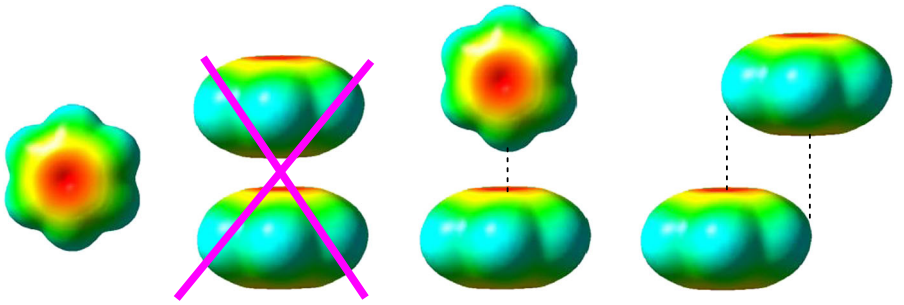

Figure 3. The electrostatic potential surfaces of benzene calculated at the M062X/6-31G(d,p) level under vacuum, where the negative electrostatic potential is in red, the positive electrostatic potential is in blue, and the green region is essentially neutral

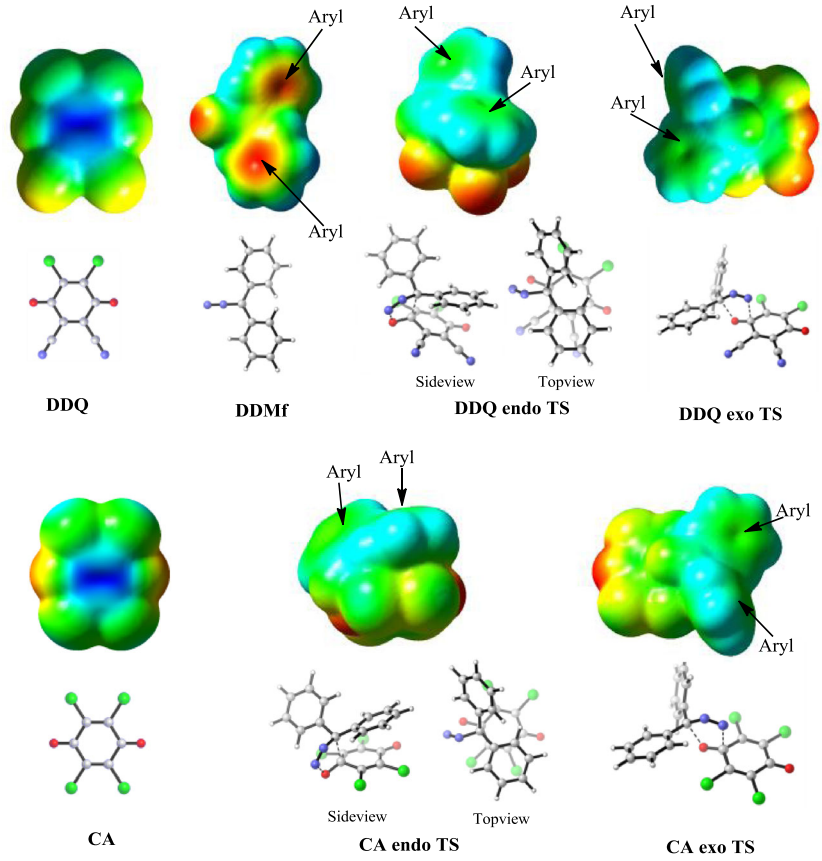

Figure 4. The electrostatic potential surfaces of DDQ, CA, and DDMf, as well as the *endo* and *exo* TS of the reactions calculated at the M06-2X/6-31G(d, p) level under vacuum, where the red region represents negative electrostatic potential, the blue one the positive electrostatic potential, and the green region is essentially neutral

Table 2. The dominant geometrical parameters for the reactants, Ints, TSs, and products in the 1,3-DPCA reactions of DDMf with C60, C70, TCNE, DDQ, and CA, as well as the only imaginary frequency of the TSs calculated at the M06-2X/6-31G(d,p) level under vacuum. (Unit: Å for bond length and cm^{-1} for frequencies)

		Reactant		Int			TS			Product		
		r_i[a]	r_i	r_1[b]	r_2[b]	r_i	r_1	r_2	v[c]	r_i	r_1	r_2
Vacuum	C_{60}	1.387	1.387	3.176	3.117	1.443	2.235	2.088	393*i*	1.578	1.612	1.508
	C_{70}	1.389	1.389	3.123	3.215	1.446	2.236	2.066	382*i*	1.580	1.613	1.507
	TCNE	1.358	1.366	3.100	2.800	1.442	2.186	2.051	347*i*	1.565	1.592	1.541
	DDQ	1.204	1.211	2.848	2.776	1.268	1.976	2.115	373*i*	1.388	1.435	1.526
	CA	1.203	1.208	3.074	2.766	1.265	1.988	2.08	401*i*	1.393	1.428	1.519
CH_3CN	C_{60}	1.387	1.387	3.178	3.113	1.444	2.219	2.085	396*i*	1.580	1.611	1.503
	C_{70}	1.389	1.389	3.114	3.135	1.445	2.243	2.055	382*i*	1.581	1.611	1.502
	TCNE	1.355	1.370	3.042	2.713	1.449	2.128	2.101	311*i*	1.571	1.485	1.602
	DDQ	1.206	1.213	2.877	2.772	1.275	1.948	2.188	320*i*	1.386	1.435	1.529
	CA	1.206	1.210	2.987	2.810	1.270	1.982	2.085	357*i*	1.429	1.392	1.484
Toluene	C_{60}	1.387	1.387	3.172	3.115	1.443	2.222	2.086	392*i*	1.578	1.612	1.506
	C_{70}	1.389	1.389	3.122	3.128	1.446	2.237	2.062	381*i*	1.580	1.612	1.505
	TCNE	1.356	1.367	3.062	2.759	1.445	2.168	2.062	328*i*	1.567	1.596	1.541
	DDQ	1.204	1.212	2.854	2.746	1.270	1.972	2.130	348*i*	1.436	1.387	1.482
	CA	1.204	1.209	3.036	2.769	1.266	1.990	2.080	381*i*	1.391	1.431	1.520

[a] r_i is the distance between the two reactive carbon atoms in C_{60}, C_{70}, and TCNE, or the distance of the attacked carbon and oxygen atoms of DDQ and CA.
[b] r_1 and r_2 are the lengths of the forming C—C and C—N single bonds during the cycloaddition of DDM with fullerenes and TCNE and the length of the forming C—O and C—N bonds during the cycloaddition of DDM with DDQ and CA.
[c] v is the imaginary frequency of the saddle point.

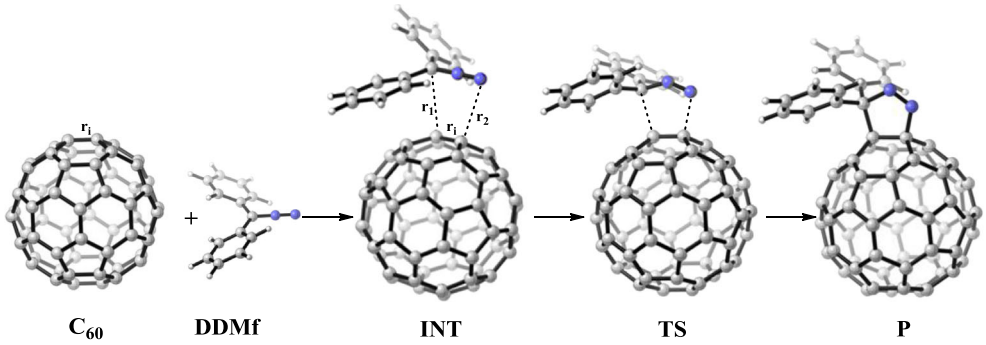

Figure 5. The reaction pathway for the 1,3-DPCA reactions of DDM on C_{60} calculated at the M06-2X/6-31G(d,p) level under vacuum. The gray, blue, and white balls represent carbon, nitrogen, and hydrogen atoms, respectively

Table 3. The ΔS, ΔH, and ΔG of the 1,3-DPCA reactions of DDMf with C_{60}, C_{70}, DDQ, TCNE, and CA calculated at the M06-2X/6-31G (d,p) level under vacuum. (Unit: kcal/mol for ΔH and ΔG, e.u. for ΔS, where e.u. = cal/(K·mol))

	Int			TS			Activation barrier			P		
	ΔS_{Int}	ΔH_{Int}	ΔG_{Int}	ΔS_{TS}	ΔH_{TS}	ΔG_{TS}	$\Delta S^{\ddagger}$	$\Delta H^{\ddagger}$	$\Delta G^{\ddagger}$	ΔS_r	ΔH_r	ΔG_r
C_{60}	−36.2	−7.0	3.8	−45.4	7.2	20.7	−9.2	14.1	16.9	−54.4	−17.1	−0.9
C_{70}	−45.1	−7.9	5.5	−48.7	6.8	21.3	−3.7	14.7	15.8	−54.6	−17.4	−1.1
TCNE	−44.0	−12.0	1.1	−51.8	0.2	15.7	−7.7	12.3	14.6	−56.1	−18.0	−1.3
DDQ	−40.8	−10.4	1.8	−50.5	0.6	15.6	−9.7	11.0	13.9	−51.5	−23.3	−7.9
CA	−33.8	−7.3	2.8	−49.6	6.7	21.5	−15.8	14.0	18.7	−47.7	−21.5	−7.2

DDQ are both the largest, indicating that the final combination is the most stable and that the driving force is the largest. Although the ΔG_r of the CA reaction is similar to that of the DDQ reaction, the high $\Delta G^{\ddagger}$ inhibits the reaction. The experiments performed in toluene at 30 °C revealed that C_{60} is approximately 1.5 times more reactive than C_{70}, and the relative reactivities of these acceptors with DDMf increased in the following order: DDQ > C_{60} ≥ C_{70} > TCNE > CA.[31] Both the calculated and experimental results indicate that DDQ has the highest reactivity but CA has the lowest reactivity with DDMf; the reactivity of C_{70} is slightly larger than that of C_{60}. The TCNE should be more reactive than the two fullerenes according to the computational results, which diverges from the experimental observations. Our thermodynamic data are derived from calculations under the standard conditions: 298.15 K and 1 atm and under vacuum. The solvent and temperature might promote the reaction of the fullerenes more than TCNE when they work together.

Distortion/interaction analysis

The distortions and interactions are depicted in Fig. 6 and listed in Table S1. For the reaction with C_{60}, 6.7 kcal/mol is required for C_{60} and 20.5 kcal/mol is required for DDMf to distort their initial structures to reach the TS. Subsequently, C_{60} and DDMf interact with each other due to the favorable orbital overlap achieved only in the geometry of the distorted state, lowering the energy of the overall system by −11.6 kcal/mol. When accounting for the distortion and interaction energies, we obtained an overall activation energy of 15.6 kcal/mol ($\Delta E^{\ddagger} = \Delta E^{\ddagger}_{dis} + \Delta E^{\ddagger}_{int}$). Compared to the reaction of DDMf with C_{60}, the total distortion energy is similar (0.7 kcal/mol lower) to that of C_{70} but 14.4, 3.1, and 4.6 kcal/mol higher for TCNE, DDQ, and CA, respectively.

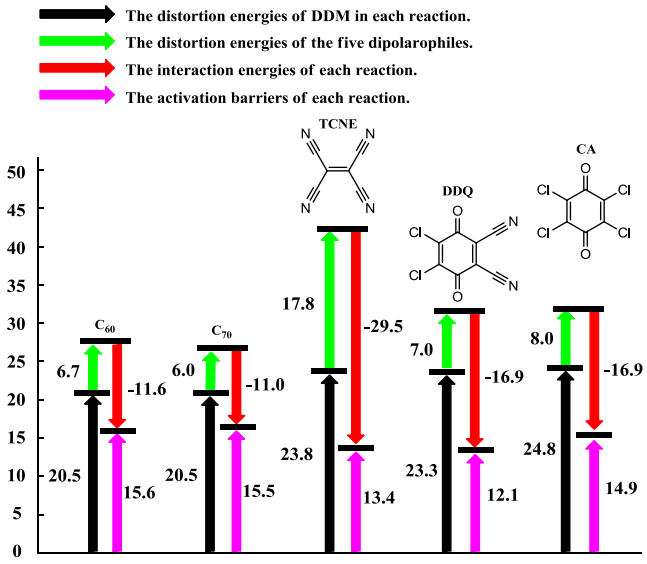

Figure 6. The distortion energies and interaction energies of the 1,3-DPCA reactions of DDMf with the five dipolarophiles at the M06-2X/6-31G(d,p) level under vacuum. The energy is in kcal/mol

The interaction energy of the C_{70} reaction is similar (0.6 kcal/mol lower) to that of the C_{60} reaction, generating a nearly identical activation energy. Despite the higher distortion barrier, the interaction energies of TCNE, DDQ, and CA are larger than that of C_{60} because a more distorted structure might generate better orbital overlap. Moreover, DDMf adds at the double carbon bond in TCNE; the overlap of the HOMO of DDMf and LUMO of TCNE is

larger than that of C_{60} and C_{70}. The difference in the interaction energies originates from the changes in the electronic structures of the reactants during the distortion process. During the reaction of DDMf with C_{60}, C_{70}, TCNE, DDQ, and CA, DDMf is a type I dipole, as characterized by Sustmann,[71–73] while C_{60}, C_{70}, DDQ, TCNE, and CA are acceptor dipolarophiles. The orbital energies of the HOMOs and LUMOs are summarized in Fig. 7.

The orbitals able to interact are the HOMO of DDMf and the LUMOs of the five dipolarophiles. Their gaps are much smaller than the gaps of the LUMO of DDMf and HOMOs of the five dipolarophiles. The HOMOs of the distorted DDMf and the LUMOs of the five acceptors are crucial to the electronic interactions.[74] From the reactant to the TS, the HOMO energy of DDMf increases from −6.35 eV to −6.25 eV, and the LUMO energy of C_{60} decreases from −2.70 eV to −2.79 eV, making the HOMO–LUMO gap smaller in the TS than in the reactants. The HOMO–LUMO gap for the C_{60} reaction is 3.46 eV. The situation is similar for the other four reactions. The gaps between the HOMO of DDMf and the LUMOs of the other four reactions are 3.39, 1.99, 1.8, and 2.67 eV for C_{70}, TCNE, DDQ, and CA in their TSs, respectively. The similar HOMO−LUMO gaps generated similar interaction energies for the C_{60} and C_{70} reactions. The very narrow HOMO−LUMO gap facilitates the electron exchange between DDMf and TCNE, validating the thermodynamic results.

Solvent effects on the five reactions

The five 1,3-DPCA reactions in toluene and CH_3CN were explored at the same theoretical level as in gas. The thermochemical data are listed in Table 4. The solvent effects barely affect ΔG_{TS} for the five reactions, and the solvent effects change $\Delta G^{\ddagger}$ slightly for the reactions with C_{60} and C_{70}. However, compared to the values under vacuum, the $\Delta G^{\ddagger}$ decreased from 1.6 to 2.1 kcal/mol in toluene and from 2.8 to 3.7 kcal/mol in CH_3CN during the other three reactions, indicating that the solvents stabilized the TS more than the reactants. The C_{60} and C_{70} reactions are more exergonic, but the other three reactions are less exergonic in the two solvents than under vacuum. In general, the solvent effects do not change the order of the reactivities for the five acceptors with DDMf and only slightly affect the five reactions, remaining consistent with the concerted mechanism. The distortion and interaction energies in the two solvents are listed in Table S1 and are depicted in Fig. 8. The solvent effects on the distortion of the C_{60} and C_{70} reactions are minor. However, the interaction energies are larger in the solvent, generating slightly lower activation energies than under vacuum for the TCNE, DDQ, and CA reactions.

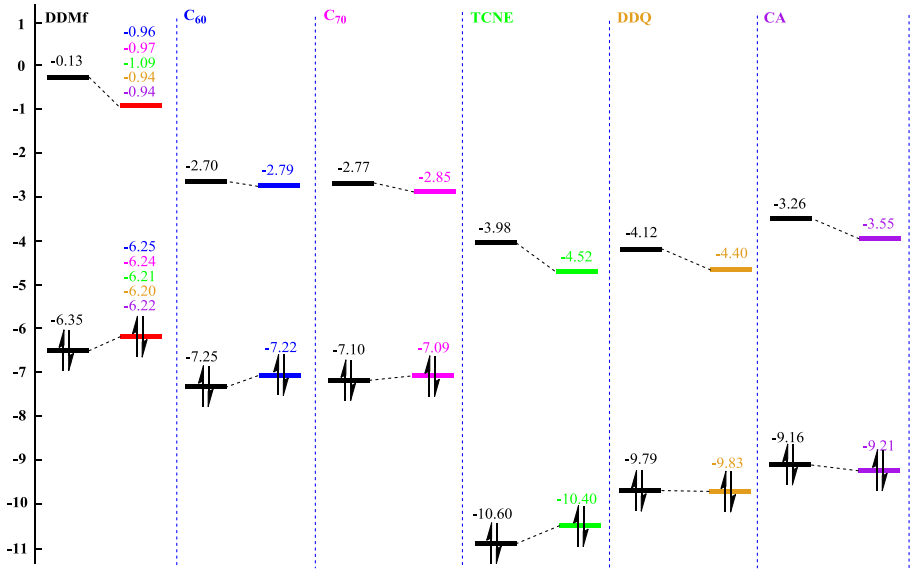

Figure 7. The HOMOs and LUMO energies of the distorted reactants in the TS, where the left columns of the six regions show the HOMO and LUMO energies of the ground states for six reactants; the right columns of each region show the HOMO and LUMO energies for the corresponding distorted structures from the five 1,3-DPCA reactions. All of the energies are calculated at the M06-2X/6-31G(d,p) level. The energy is in eV

The 1,3-DPCA reactions of DDMs with the five acceptors

Many efforts have been made to uncover the substituent effects on the reactivity of fullerenes in recent years. Keshavarz-K et al. compared the effects of the electron donating and withdrawing substituents on methanofullerene (C_{61}) and found that the cyano group exerted a stronger electron withdrawing ability than was predicted by the Hammett relation.[75] Bagno's group quantitatively reported the substituent effects of the dihydro [60]fullerenyl group and its hydrophobic parameters.[76] The substituent effect is the manner in which the reactivity of the molecule varies with the substituents. Studies of substituent effects are crucial when investigating organic reaction mechanisms involving fullerenes. The goal of changing substituents is to determine how that change affects the equilibrium for the reaction or the activation free energy and therefore the structure of the activated complex. Substituent effects are often discussed in terms of five effects: field, resonance, inductive, polarization, and steric effects. The first four effects are all electronic effects, while the steric effects depend primarily on the size of the substituent.

To study the substituent effects on the five current reactions, the 1,3-DPCA reactions of the 12 substituted DDMf with each of the five dipolarophiles are investigated at the M06-2X/6-31G(d,p) theoretical level. When combined with the five reactions with DDMf in Section 3.1, 65 reactions are analyzed in the current study. The substituent groups (Fig. 1) in the 12 DDMf derivatives can be divided into two types: electron-donating groups (EDG), such as -MeO and -Me, and electron-withdrawing groups (EWG), such as -Cl, $-CF_3$, and $-NO_2$. The reactions of the five dipolarophiles with the substituted DDMs have a similar mechanism to their reactions with the unsubstituted DDMf. We located an Int for each of the 60 reactions. The geometries of the Ints, reactants, TSs, and products are listed in Table S2. The Cartesian coordinates of these structures are listed in the supplementary data. The r_1 and r_2 of these reactions are different for the TSs and products, suggesting that all of the reactions are asynchronous. The ΔS^{TS}, $\Delta S^{\ddagger}$, and ΔS_r; ΔH^{TS}, $\Delta H^{\ddagger}$, and ΔH_r; and ΔG^{TS}, $\Delta G^{\ddagger}$,

Table 4. The ΔS, ΔH, and ΔG of the 1,3-DPCA reactions of DDMf with C_{60}, C_{70}, TCNE, DDQ, and CA calculated at the M06-2X/6-31G (d,p) level in toluene and CH_3CN. (Unit: kcal/mol for ΔH and ΔG, e.u. for ΔS, where e.u. = cal/(K·mol))

		Int			TS			Activation barrier			P		
		ΔS_{int}	ΔH_{int}	ΔG_{int}	ΔS_{TS}	ΔH_{TS}	ΔG_{TS}	$\Delta S^{‡}$	$\Delta H^{‡}$	$\Delta G^{‡}$	ΔS_r	ΔH_r	ΔG_r
Toluene	C_{60}	−37.0	−6.8	4.2	−48.0	6.9	21.2	−11.0	13.7	17.0	−54.4	−17.9	−1.7
	C_{70}	−45.4	−7.4	6.1	−47.8	6.8	21.1	−2.3	14.3	15.0	−53.3	−17.9	−2.0
	TCNE	−46.3	−11.3	2.5	−53.3	−0.8	15.1	−7.0	10.4	12.5	−56.5	−17.7	−0.9
	DDQ	−40.3	−9.2	2.8	−51.2	0.5	15.7	−10.9	9.7	12.9	−53.0	−22.1	−6.3
	CA	−35.8	−6.4	4.3	−50.3	6.4	21.4	−14.5	12.8	17.1	−51.6	−20.4	−5.0
CH_3CN	C_{60}	−36.9	−6.5	4.5	−47.6	6.8	21.0	−10.7	13.3	16.5	−53.7	−19.8	−3.8
	C_{70}	−43.6	−7.1	5.9	−48.6	6.6	21.1	−5.0	13.7	15.2	−53.7	−19.8	−3.8
	TCNE	−44.5	−10.9	2.4	−51.5	−1.8	13.6	−7.0	9.2	11.2	−56.3	−17.1	−0.3
	DDQ	−42.3	−7.6	5.0	−50.9	1.0	16.2	−8.6	8.6	11.1	−52.2	−20.5	−4.9
	CA	−40.4	−5.6	6.5	−49.8	6.6	21.5	−9.4	12.2	15.0	−50.4	−19.0	−4.0

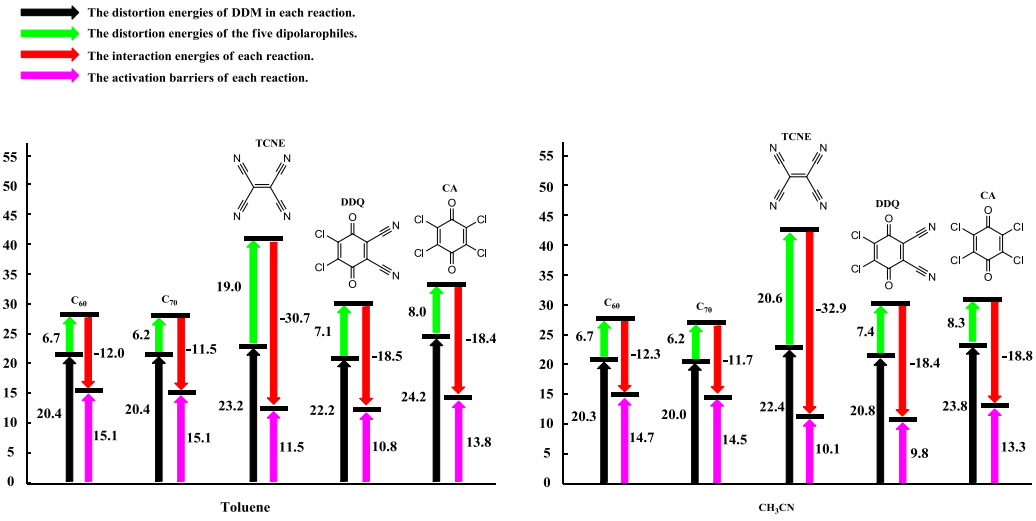

Figure 8. The distortion and interaction energies of the 1,3-DPCA reactions of DDMf with the five dipolarophiles calculated at the M06-2X/6-31G(d,p) level in toluene and CH_3CN. The energy is in kcal/mol

and ΔG_r are tabulated in Table S3. According to the thermochemical data, EWGs often increase the $\Delta G^{‡}$, while EDGs often decrease $\Delta G^{‡}$ because DDM is the electron donating reactant and the five dipolarophiles are electron receptors. As shown in Table S4, the EDGs donate electron density to the reaction center of one carbon and two nitrogen atoms, increasing the energy of the DDM HOMO to approach the LUMO of the five receptors and facilitating the reactions. In contrast, EDGs exert an inverse effect, adversely affecting the reactions. Figure S3 shows the electrostatic potential surfaces of the 13 DDMs. The two phenyl rings have negative electronic potential from DDMa to DDMj and positive electronic potential in DDMk, DDMl, and DDMm. As shown in Fig. 4, the centers of DDQ and CA have a positive electronic potential, which repulses the phenyl rings from DDMk to DDMm, increasing the $\Delta G^{‡}$s for the three reactions.

Consideration of a biradical mechanism

To investigate a possible biradical mechanism for the 1,3-DPCA reactions of DDMf with fullerenes, we employed an unrestricted M06-2X functional with a broken symmetry technique. During the optimizations, we let the two C=C bonds of butadiene rotate freely around the middle C—C bond; however, the originally designed structure of biradical TSs will revert to the structure utilizing the concerted pathways during all of the reactions. Therefore, the biradical pathway is not available to these reactions.

CONCLUSION

We theoretically investigated 65 1,3-DPCA reactions of diphenyldiazomethanes with C_{60} and C_{70}, TCNE, DDQ, and CA based on the M06-2X/6-31G(d,p) calculations. The stereoselectivity, solvent effects, and substituent effects were discussed based on analyses of the distortion-interaction model, electronic structure, solvent model, and thermodynamic data. The calculated results agree with and enrich the experimental observations. The present calculations indicated the following: (i) the *exo* pathway is more favorable for the reactions of DDMf with DDQ (or CA) due to steric and thermodynamic effects; (ii) the 1,3-DPCA reaction is a prototypical "no-mechanism" pericyclic reaction. However, one Int was located between the reactant and the TS for all 65 of the 1,3-DPCA reactions; (iii) the distortion of the

reactants toward their structures in the TS is a hindering factor, but the interaction energy promotes the reaction. In addition, the HOMO–LUMO gap has a direct relationship with the interaction energy; (iv) solvents such as toluene and CH_3CN have a minor impact on the reaction energy profile as well as the distortion and interaction energies for the five unsubstituted reactions; (v) EDGs promote and EWGs hinder the five unsubstituted reactions; and (vi) a biradical pathway for the reactions of DDMf with the two fullerenes is unlikely.

Acknowledgements

This study was supported by grants from the National Nature Science Foundation of China (Grant Nos. 21273021 and 21325312) and the Major State Basic Research Development Programs (Grant No. 2011CB808500).

REFERENCES

[1] S. H. Friedman, D. L. DeCamp, R. P. Sijbesma, G. Srdanov, F. Wudl, G. L. Kenyon, *J. Am. Chem. Soc.* **1993**, *115*, 6506–6509.
[2] S. H. Friedman, P. S. Ganapathi, Y. Rubin, G. L. Kenyon, *J. Med. Chem.* **1998**, *41*, 2424–2429.
[3] A. W. Jensen, S. R. Wilson, D. I. Schuster, *Bioorg. Med. Chem.* **1996**, *4*, 767–779.
[4] K. M. Coakley, M. D. McGehee, *Chem. Mater.* **2004**, *16*, 4533–4542.
[5] L. M. Giovane, J. W. Barco, T. Yadav, A. L. Lafleur, J. A. Marr, J. B. Howard, V. M. Rotello, *J. Phys. Chem.* **1993**, *97*, 8560–8561.
[6] K. Hedberg, L. Hedberg, D. S. Bethune, C. A. Brown, H. C. Dorn, R. D. Johnson, M. De Vries, *Science* **1991**, *254*, 410.
[7] A. Chikama, H. Fueno, H. Fujimoto, *J. Phys. Chem.* **1995**, *99*, 8541–8549.
[8] A. L. Balch, V. J. Catalano, J. W. Lee, M. M. Olmstead, S. R. Parkin, *J. Am. Chem. Soc.* **1991**, *113*, 8953–8954.
[9] G. Scuseria, *Chem. Phys. Lett.* **1991**, *180*, 451–456.
[10] B. Illescas, N. Martín, C. Seoane, P. de la Cruz, F. Langa, F. Wudl, *Tetrahedron Lett.* **1995**, *36*, 8307–8310.
[11] S. I. Osuna, J. Morera, M. Cases, K. Morokuma, M. Solà, *J. Phys. Chem. A* **2009**, *113*, 9721–9726.
[12] M. Prato, V. Lucchini, M. Maggini, E. Stimpfl, G. Scorrano, M. Eiermann, T. Suzuki, F. Wudl, *J. Am. Chem. Soc.* **1993**, *115*, 1148–1150.
[13] Y. Rubin, S. Khan, D. I. Freedberg, C. Yeretzian, *J. Am. Chem. Soc.* **1993**, *115*, 344–345.
[14] X. Xu, Z. Shang, R. Li, Z. Cai, X. Zhao, *J. Mol. Struc.:Theochem* **2008**, *864*, 6–13.
[15] K. L. Wooley, C. J. Hawker, J. M. J. Frechet, F. Wudl, G. Srdanov, S. Shi, C. Li, M. Kao, *J. Am. Chem. Soc.* **1993**, *115*, 9836–9837.
[16] T. Suzuki, Q. Li, K. C. Khemani, F. Wudl, *J. Am. Chem. Soc.* **1992**, *114*, 7301–7302.
[17] A. B. Smith, R. M. Strongin, L. Brard, G. T. Furst, W. J. Romanow, K. G. Owens, R. C. King, *J. Am. Chem. Soc.* **1993**, *115*, 5829–5830.
[18] S. Shi, K. C. Khemani, Q. Li, F. Wudl, *J. Am. Chem. Soc.* **1992**, *114*, 10656–10657.
[19] G. Schick, A. Hirsch, *Tetrahedron* **1998**, *54*, 4283–4296.
[20] M. Prato, Q. C. Li, F. Wudl, V. Lucchini, *J. Am. Chem. Soc.* **1993**, *115*, 1148–1150.
[21] Z. Li, P. B. Shevlin, *J. Am. Chem. Soc.* **1997**, *119*, 1149–1150.
[22] Z. Li, K. H. Bouhadir, P. B. Shevlin, *Tetrahedron Lett.* **1996**, *37*, 4651–4654.
[23] T. Ishida, K. Shinozuka, T. Nogami, M. Kubota, M. Ohashi, *Tetrahedron* **1996**, *52*, 5103–5112.
[24] J. C. Hummelen, B. W. Knight, F. LePeq, F. Wudl, J. Yao, C. L. Wilkins, *J. Org. Chem.* **1995**, *60*, 532–538.
[25] M. H. Hall, H. Lu, P. B. Shevlin, *J. Am. Chem. Soc.* **2001**, *123*, 1349–1354.
[26] M. Sola, M. Duran, J. Mestres, *J. Am. Chem. Soc.* **1996**, *118*, 8920–8924.
[27] J. H. Sheu, M. D. Su, *Chem. Eur. J.* **2007**, *13*, 6171–6178.
[28] C. C. Henderson, M. M. Rohlfing, *Chem. Phys. Lett.* **1993**, *213*, 383–388.
[29] H. Isobe, T. Tanaka, W. Nakanishi, L. Lemiegre, E. Nakamura, *J. Org. Chem.* **2005**, *70*, 4826–4832.
[30] T. Ishi-i, K. Nakashima, S. Shinkai, *Chem. Commun.* **1998**, *9*, 1047–1048.
[31] T. Oshima, H. Kitamura, T. Higashi, K. Kokubo, N. Seike, *J. Org. Chem.* **2006**, *71*, 2995–3000.
[32] Y. Ueno, S. Saito, *Physica E* **2007**, *40*, 285–288.
[33] S. Bhattacharya, T. Shimawaki, X. Peng, A. Ashokkumar, S. Aonuma, T. Kimura, N. Komatsu, *Chem. Phys. Lett.* **2006**, *430*, 435–442.
[34] V. Schettino, M. Pagliai, G. Cardini, *J. Phys. Chem. A* **2002**, *106*, 1815–1823.
[35] X. Lu, F. Tian, Y. Feng, X. Xu, N. Wang, Q. Zhang, *Nano Lett.* **2002**, *2*, 1325–1327.
[36] E. Goldstein, B. Beno, K. Houk, *J. Am. Chem. Soc.* **1996**, *118*, 6036–6043.
[37] B. Jursic, Z. Zdravkovski, *J. Chem. Soc., Perkin Trans. 2* **1995**, 1223–1226.
[38] V. Barone, R. Arnaud, *J. Chem. Phys.* **1997**, *106*, 8727–8732.
[39] B. Beno, K. Houk, D. Singleton, *J. Am. Chem. Soc.* **1996**, *118*, 9984–9985.
[40] M. Petrukhina, K. Andreini, J. Mack, L. Scott, *J. Org. Chem.* **2005**, *70*, 5713–5716.
[41] S. N. Pieniazek, F. R. Clemente, K. N. Houk, *Angew. Chem. Int. Ed.* **2008**, *47*, 7746–7749.
[42] T. Heaton-Burgess, W. Yang, *J. Chem. Phys.* **2010**, *132*, 4113.
[43] Y. Zhao, D. G. Truhlar, *Theor. Chem. Account.* **2008**, *120*, 215–241.
[44] S. A. Lopez, M. E. Munk, K. N. Houk, *J. Org. Chem.* **2013**, *78*, 1576–1582.
[45] Y. Lan, S. E. Wheeler, K. N. Houk, *J. Chem. Theory Comput.* **2011**, *7*, 2104–2111.
[46] E. H. Krenske, K. N. Houk, A. B. Holmes, J. Thompson, *Tetrahedron Lett.* **2011**, *52*, 2181–2184.
[47] X.-F. Gao, C.-X. Cui, Y.-J. Liu, *J. Phys. Org. Chem.* **2012**, *25*, 850–855.
[48] D. H. Ess, K. N. Houk, *J. Am. Chem. Soc.* **2007**, *129*, 10646–10647.
[49] Y. Lan, K. N. Houk, *J. Am. Chem. Soc.* **2010**, *132*, 17921–17927.
[50] S. Liu, Y. Lei, X. Qi, Y. Lan, *J. Phys. Chem. A* **2014**, *118*, 2638–2645.
[51] F. Liu, R. S. Paton, S. Kim, Y. Liang, K. N. Houk, *J. Am. Chem. Soc.* **2013**, *135*, 15642–15649.
[52] L. R. Domingo, J. A. Saez, J. A. Joule, L. Rhyman, P. Ramasami, *J. Org. Chem.* **2013**, *78*, 1621–1629.
[53] C. G. Gordon, J. L. Mackey, J. C. Jewett, E. M. Sletten, K. N. Houk, C. R. Bertozzi, *J. Am. Chem. Soc.* **2012**, *134*, 9199–9208.
[54] A. C. Knall, C. Slugovc, *Chem. Soc. Rev.* **2013**, *42*, 5131–5142.
[55] Y. Liang, J. L. Mackey, S. A. Lopez, F. Liu, K. N. Houk, *J. Am. Chem. Soc.* **2012**, *134*, 17904–17907.
[56] F. Schoenebeck, K. N. Houk, *J. Am. Chem. Soc.* **2010**, *132*, 2496–2497.
[57] F. M. Bickelhaupt, *J. Comput. Chem.* **1999**, *20*, 114–128.
[58] G. T. de Jong, F. M. Bickelhaupt, *ChemPhysChem* **2007**, *8*, 1170–1181.
[59] A. Diefenbach, F. M. Bickelhaupt, *J. Chem. Phys.* **2001**, *115*, 4030–4040.
[60] A. Diefenbach, G. T. de Jong, F. M. Bickelhaupt, *J. Chem. Theory Comput.* **2005**, *1*, 286–298.
[61] W.-J. van Zeist, F. M. Bickelhaupt, *Org. Biomol. Chem.* **2010**, *8*, 3118–3127.
[62] Y. Lan, L. Zou, Y. Cao, K. N. Houk, *J. Phys. Chem. A* **2011**, *115*, 13906–13920.
[63] W. J. Hehre, L. Radom, P. v. R. Schleyer, J. A. Pople, *Ab initio molecular theory*, John Wiley, New York, **1986**.
[64] J. Tomasi, M. Persico, *Chem. Rev.* **1994**, *94*, 2027–2094.
[65] V. Barone, M. Cossi, *J. Phys. Chem. A* **1998**, *102*, 1995–2001.
[66] M. Cossi, N. Rega, G. Scalmani, V. Barone, *J. Comput. Chem.* **2003**, *24*, 669–681.
[67] M. J. Frisch, G. W. Trucks, H. B. Schlegel, G. E. Scuseria, M. A. Robb, J. R. Cheeseman, G. Scalmani, V. Barone, B. Mennucci, G. A. Petersson, H. Nakatsuji, M. Caricato, X. Li, H. P. Hratchian, A. F. Izmaylov, J. Bloino, G. Zheng, J. L. Sonnenberg, M. Hada, M. Ehara, K. Toyota, R. Fukuda, J. Hasegawa, M. Ishida, T. Nakajima, Y. Honda, O. Kitao, H. Nakai, T. Vreven, J. A. Montgomery, Jr., J. E. Peralta, F. Ogliaro, M. Bearpark, J. J. Heyd, E. Brothers, K. N. Kudin, V. N. Staroverov, R. Kobayashi, J. Normand, K. Raghavachari, A. Rendell, J. C. Burant, S. S. Iyengar, J. Tomasi, M. Cossi, N. Rega, J. M. Millam, M. Klene, J. E. Knox, J. B. Cross, V. Bakken, C. Adamo, J. Jaramillo, R. Gomperts, R. E. Stratmann, O. Yazyev, A. J. Austin, R. Cammi, C. Pomelli, J. W. Ochterski, R. L. Martin, K. Morokuma, V. G. Zakrzewski, G. A. Voth, P. Salvador, J. J. Dannenberg, S. Dapprich, A. D. Daniels, O. Farkas,

J. B. Foresman, J. V. Ortiz, J. Cioslowski, D. J. Fox, *Gaussian 09, Revision A.02*, Gaussian, Inc., Wallingford CT, **2009**.
[68] T. Oshima, T. Nagai, *Bull. Chem. Soc. Jpn.* **1981**, *54*, 2039–2044.
[69] T. Oshima, T. Nagai, *Bull. Chem. Soc. Jpn.* **1980**, *53*, 3284–3288.
[70] T. Oshima, A. Yoshioka, T. Nagai, *J. Chem. Soc., Perkin Trans. 2* **1978**, 1283–1287.
[71] R. Sustmann, *Tetrahedron Lett.* **1971**, *12*, 2717–2720.
[72] R. Sustmann, H. Trill, *Angew. Chem. Int. Ed.* **1972**, *11*, 838–840.
[73] R. Sustmann, *Pure Appl. Chem.* **1974**, *40*, 569–593.
[74] A. S. Lobach, V. V. Strelets, *Russ. Chem. Bull.* **2001**, *50*, 1593–1595.
[75] M. Keshavarz-K, B. Knight, R. C. Haddon, F. Wudl, *Tetrahedron* **1996**, *52*, 5149–5159.
[76] A. Bagno, S. Claeson, M. Maggini, M. L. Martini, M. Prato, G. Scorrano, *Chem. Eur. J.* **2002**, *8*, 1015–1023.

SUPPORTING INFORMATION

Additional supporting information may be found in the online version of this article at the publisher's website.